Molecular Crystals and Liquid Crystals

ISSN: 1542-1406 (Print) 1563-5287 (Online) Journal homepage: http://www.tandfonline.com/loi/gmcl20

# Theoretical Investigation on the Electronic Structures and Optoelectronic Properties of a Series of Platinum(II) Complexes with Different Substituent Groups

Deming Han, Jingmei Li, Chunying Pang, Lihui Zhao, Bing Xia & Gang Zhang

**To cite this article:** Deming Han, Jingmei Li, Chunying Pang, Lihui Zhao, Bing Xia & Gang Zhang (2015) Theoretical Investigation on the Electronic Structures and Optoelectronic Properties of a Series of Platinum(II) Complexes with Different Substituent Groups, Molecular Crystals and Liquid Crystals, 616:1, 133-142, DOI: 10.1080/15421406.2014.954317

**To link to this article:** http://dx.doi.org/10.1080/15421406.2014.954317

*Mol. Cryst. Liq. Cryst.*, Vol. 616: pp. 133–142, 2015

ISSN: 1542-1406 print/1563-5287 online
DOI: 10.1080/15421406.2014.954317



# Theoretical Investigation on the Electronic Structures and Optoelectronic Properties of a Series of Platinum(II) Complexes with Different Substituent Groups

DEMING HAN,[1] JINGMEI LI,[1] CHUNYING PANG,[1] LIHUI ZHAO,[1] BING XIA,[1,*] AND GANG ZHANG[2]

[1]School of Life Science and Technology, Changchun University of Science and Technology, Changchun, Jilin, P. R. China
[2]State Key Laboratory of Theoretical and Computational Chemistry, Institute of Theoretical Chemistry, Jilin University, Changchun, Jilin, P. R. China

*A theoretical investigation was performed on a series of platinum(II) complexes with the dipivaloylmethane as ancillary ligand and tetrahydroquinolines with different substituent group (–$CF_3$, –CN, –H, –$CH_3$, and –$OCH_3$) as C^N cyclometalating ligand. The geometry structures, electronic structures, absorption, and phosphorescent properties of these platinum(II) complexes have been investigated. Ionization potential and electron affinity were calculated to evaluate the injection abilities of holes and electrons into these complexes. The lowest energy absorption wavelengths are located at 362 nm for* ***1****, 372 nm for* ***2****, 361 nm for* ***3****, 361 nm for* ***4****, and 355 nm for* ***5****, respectively. The lowest energy emissions of these complexes are localized at 520, 544, 513, 519, and 523 nm, respectively, for complexes* ***1****–****5****, simulated in $CH_2Cl_2$ medium at M062X level. The calculated results indicate that the complex* ***2*** *possibly possesses the largest $k_r$ value among the five complexes. It is expected that the study can be useful for designing and synthesizing the new phosphorescent OLEDs materials.*

**Keywords** DFT; TDDFT; emission, platinum; phosphorescence

## 1. Introduction

In the past two decades, phosphorescent transition metal complexes have attracted great attention due to their excellent photophysical properties and applications in the fabrication of organic light-emitting diodes (OLEDs) [1–5]. Iridium(III), platinum(II), osmium(II), and ruthenium(II) ions are highly effective for triggering phosphorescent emission by spin–orbit coupling, which constructs the phosphorescent triplet emitters by chelating transition metal ions with organic ligands [6–9]. These metals complexes can use both the singlet and triplet excitons when incorporated into OLEDs, which can achieve a maximum internal quantum efficiency (IQE) of 100% [10]. It is known that phosphorescent Pt(II) complexes

*Address correspondence to Bing Xia, School of Life Science and Technology, Changchun University of Science and Technology, Changchun 130022, Jilin, P. R. China. E-mail: xiabingcust2007@163.com

Color versions of one or more of the figures in the article can be found online at www.tandfonline.com/gmcl.

as OLEDs material have been extensively investigated, which the square-planar structure of the Pt(II) complex is beneficial to the electron delocalization and electron-hole creation and separation. In 1998, Baldo et al. [11] applied the phosphorescent-dopant platinum octaethylporphine in the OLEDs to harvest triplet excitons, which breaks the 25% theoretical IQE limitation predicted in fluorescent devices based on singlet exciton emission. Much work on cyclometalated Pt(II) complexes based on NˆNˆC-coordinating ligands and their emitting characteristics have been reported by Che et al. [12,13]. Y. Unger et al. [14] prepared some homoleptic Pt(II) biscarbene complexes which were emissive in the deep blue region. Recently, K. Feng et al. [15] reported some interesting Pt phosphors with bridged ligands and their copolymers. These platinum complexes exhibit peak emissions around 525 nm with a maximum ΦP around 0.55 in degassed $CH_2Cl_2$ and their corresponding polymers display almost identical photoluminescence spectra in poly(*N*-vinylcarbazole) (PVK) films. The luminescence properties of heteroleptic CˆN cyclometalated complexes with the general formula [Pt(CˆN)(OˆO)] have been studied, and some of these promising emitter molecules were used in OLEDs [16–21]. Based on the Pt(II) complexes with bidentate cyclometalated aryl pyridine ligands and acetylacetonate auxiliary ligands, a lot of variations regarding substituents, size of the $\pi$ systems, heterocycles, and auxiliary ligands were investigated to tune the photophysical properties [22].

It is known that the photophysical properties of Pt(II) complexes are affected by the modification of the ligands via attaching electron-donating/withdrawing groups. In this study, five platinum(II) complexes with the dipivaloylmethane as ancillary ligand and tetrahydroquinolines with different substituent group (–$CF_3$, –CN, –H, –$CH_3$, and –$OCH_3$) as CˆN cyclometalating ligand have been investigated using the density functional theory (DFT) and time-dependent density functional theory (TDDFT). Comparison of electronic structures and spectral properties for the five platinum(II) complexes was carried out. The research work is anticipated to provide the guidance for synthesizing and designing novel platinum-based phosphors with great potential application for electroluminescent materials.

## 2. Computational Details

The ground state geometry for each molecule was optimized by the DFT method with hybrid Hartree-Fock/density functional model (PBE0) based on the Perdew-Burke-Erzenrhof (PBE) [23]. The geometry optimizations of the lowest triplet states ($T_1$) were performed by PBE0 approach. On the basis of the ground- and excited-state equilibrium geometries, the TDDFT approach associated with the polarized continuum model in dichloromethane ($CH_2Cl_2$) medium was applied to investigate the absorption and emission spectral properties. The LANL2DZ and 6–31G(d) basis sets were used for the Pt atom and the other atoms, respectively. Furthermore, the stable configurations of these complexes can be confirmed by frequency analysis, in which no imaginary frequency was found for all configurations at the energy minima. In addition, the positive and negative ions with regard to the "electron-hole" creation are relevant to their use as OLEDs materials. Thus, ionization potentials (IP), electron affinities (EA), and reorganization energy ($\lambda$) were obtained by comparing the energy levels of neutral molecule with positive ions and negative ions, respectively. The calculated electronic density plots for frontier molecular orbitals were prepared by using the GaussView 5.0.8 software. The simulated absorption spectra are obtained by using the GaussSum 2.5 software [24]. All calculations were performed with the Gaussian 09 software package [25].

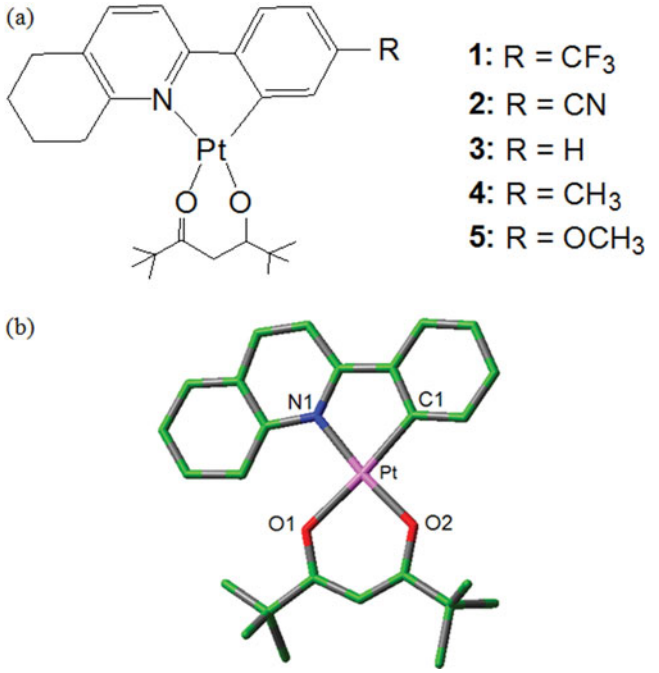


**Figure 1.** (a) Sketch map of the structures of platinum(II) complexes **1**–**5.** (b) Representative optimized structure of **3** (H atoms omitted).

## 3. Results and Discussion

### *3.1. Geometries in the Ground State $S_0$ and Triplet Excited State $T_1$*

The sketch map of the five complexes **1**, **2**, **3**, **4**, and **5** are presented in Fig. 1(a), and the optimized ground state geometric structure for **4** is shown in Fig. 1(b) along with the numbering of some key atoms. In order to verify the reliability of the calculation method, the structure parameters of complexes **1** and **3** computed with PBE0 and B3LYP methods have were compared with the experimental results (X-ray crystal structure data). It can be seen that a good agreement with experimental data was obtained for DFT/PBE0 method with 6–31G(d) basis sets. Hence, PBE0 method is adopted to study these complexes. For the studied complexes, the selected optimized geometry parameters together with the available X-ray crystal structure data for **1** [26] are given in Table 1.

These platinum(II) complexes have the dipivaloylmethane as ancillary ligand and tetrahydroquinolines with different substituent group (–$CF_3$, –CN, –H, –$CH_3$, and –$OCH_3$) as CˆN cyclometalating ligand. From the Table 1, it can be seen that the bond distances of Pt-N1 for these complexes in the ground state $S_0$ are obviously larger than that of Pt-C1, which has the same conclusion to compare the bond distances of Pt-O1 with that of Pt-O2. All these complexes show the planarity as dihedral angles of C1-N1-O1-O2 are less than 4º.

On the whole, for the triplet excited state $T_1$, the bond distances are shorter for Pt–C1, Pt–N1 and Pt–O1 bonds and longer for Pt–O2 bonds compared with those in the singlet state ($S_0$). Meanwhile, the bond angles C1-Pt-N1, O1-Pt-O2, and N1-Pt-O2 and the

**Table 1.** Main optimized geometry parameters for complexes **1–5**

| | 1 | | 2 | | 3 | | 4 | | 5 | |
|---|---|---|---|---|---|---|---|---|---|---|
| | $S_0$ | $T_1$ | $S_0$ | $T_1$ | $S_0$ | $T_1$ | $S_0$ | $T_1$ | $S_0$ | $T_1$ |
| Bond length (Å) | | | | | | | | | | |
| Pt-C1 | 1.9644 | 1.9337 | 1.9668 | 1.9405 | 1.9691 | 1.9448 | 1.9698 | 1.9476 | 1.9684 | 1.9579 |
| Pt-N1 | 2.0658 | 2.0319 | 2.0584 | 2.0361 | 2.0520 | 2.0186 | 2.0596 | 2.0181 | 2.0558 | 2.0136 |
| Pt-O1 | 2.1602 | 2.1469 | 2.1548 | 2.1490 | 2.1644 | 2.1587 | 2.1693 | 2.1588 | 2.1614 | 2.1560 |
| Pt-O2 | 2.0239 | 2.0380 | 2.0233 | 2.0345 | 2.0267 | 2.0407 | 2.0276 | 2.0402 | 2.0260 | 2.0354 |
| Bond angle (°) | | | | | | | | | | |
| C1-Pt-N1 | 80.96 | 82.23 | 81.02 | 82.31 | 81.13 | 82.28 | 81.11 | 82.25 | 81.22 | 82.16 |
| O1-Pt-O2 | 85.93 | 86.97 | 86.40 | 86.83 | 86.33 | 86.84 | 85.78 | 86.82 | 86.42 | 87.17 |
| C1-Pt-O1 | 174.93 | 172.80 | 174.54 | 173.59 | 174.06 | 173.81 | 174.68 | 173.89 | 174.24 | 174.49 |
| N1-Pt-O2 | 170.31 | 172.58 | 170.96 | 172.51 | 171.56 | 172.95 | 171.21 | 173.02 | 171.31 | 172.55 |
| Dihedral angle (°) | | | | | | | | | | |
| C1-N1-O1-O2 | 1.29 | 4.92 | 2.62 | 4.10 | 3.21 | 4.17 | 2.20 | 4.08 | 2.87 | 3.26 |

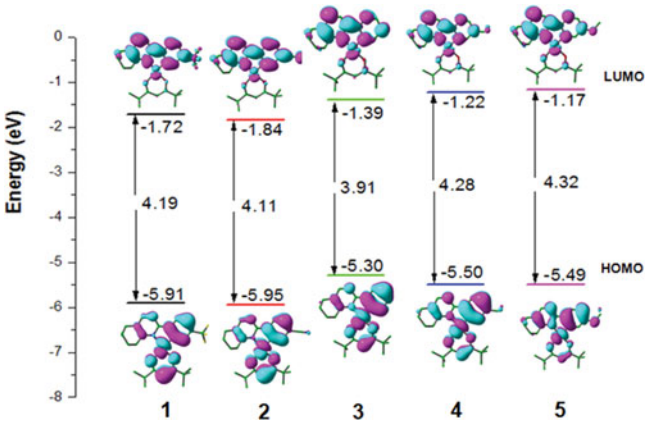


**Figure 2.** Molecular orbital diagrams and HOMO and LUMO energies for complexes **1**–**5**.

dihedral angle C1-N1-O1-O2 in the $T_1$ state for these complexes show obvious increase in comparison to those in the $S_0$ state.

### *3.2. Molecular Orbital Properties*

It is known that the concept of emission color tuning by grafting electronactive substituents relies on the fact that the lowest excited state is often relatively well described as a HOMO to LUMO transition in a given ligand [27]. The HOMO and LUMO distribution, energy levels, and energy gaps between of LUMO and HOMO ($\Delta E_{L\rightarrow H}$) of the five complexes **1**–**5** are plotted in Fig. 2. The calculated FMOs compositions for **1**–**5** were listed in Tables S1–S5 (Supplemental material).

It can be seen from Fig. 2 that the electronic cloud distribution of HOMO for complexes **1** and **2** averagely localized on the whole complex. For example, the HOMO of **1** is mainly composed of 33% metal Pt(II) d orbital, 33% C^N moiety, and 34% dpmH moiety. In addition, the electronic cloud of HOMO for complexes **3**–**5** show main distribution on the Pt(II) d orbital and C^N moiety. For example, the HOMO of **5** is mainly composed of 20% metal Pt(II) d orbital and 75% C^N moiety. It can be also seen that the electronic cloud distribution LUMO of complexes **1**–**5** are similar and mostly located on the C^N moiety. For example, the LUMO of **1** mostly located on the C^N moiety. The $\Delta E_{L\rightarrow H}$ value (3.91 eV) of complex **3** is the smallest among these complexes studied. Compared with **3**, complexes **1** and **2** with different electron-withdrawing substituents ($CF_3$ and CN) in the ancillary ligand have the smaller HOMO and LUMO energies. However, complexes **4** and **5** have the smaller HOMO and larger LUMO energies than those of **3**. Compared with that of the complex **3**, the decreased LUMO energy levels of complexes **1** and **2** will benefit the electron injection, whereas the decreased HOMO levels will weaken the hole injection ability.

### *3.3. Ionization Potential (IP) and Electronic Affinity (EA)*

It is known that the device performance of OLEDs depends on the charge injection, transfer, and balance as well as the exciton confinement in a device. Herein, we calculate vertical ionization potentials ($IP_v$), adiabatic ionization potentials ($IP_a$), vertical electron affinities

**Table 2.** The calculated vertical IP ($IP_v$), adiabatic IP ($IP_a$), hole extraction potential (HEP), vertical EA ($EA_v$), and adiabatic EA ($EA_a$), electron extraction potential (EEP), and reorganization energies for electron ($\lambda_{electron}$) and hole ($\lambda_{hole}$), unit: eV

| | $IP_v$ | $IP_a$ | $EA_v$ | $EA_a$ | HEP | EEP | $\lambda_{electron}$ | $\lambda_{hole}$ |
|---|---|---|---|---|---|---|---|---|
| 1 | 7.118 | 7.000 | 0.482 | 0.676 | 6.848 | 0.871 | 0.389 | 0.269 |
| 2 | 7.136 | 7.035 | 0.623 | 0.781 | 6.896 | 0.942 | 0.318 | 0.240 |
| 3 | 6.754 | 6.642 | 0.073 | 0.207 | 6.525 | 0.322 | 0.249 | 0.228 |
| 4 | 6.718 | 6.594 | 0.004 | 0.137 | 6.466 | 0.282 | 0.278 | 0.252 |
| 5 | 6.702 | 6.588 | 0.042 | 0.092 | 6.461 | 0.246 | 0.288 | 0.241 |



($EA_v$), adiabatic electron affinities ($EA_a$), hole extraction potential (HEP), and electron extraction potential (EEP).

In Table 2, the IP value of complex **5** is the smallest one, which means that the hole injection is much easier in complex **5** than others. The EA values of complexes **1** and **2** are obviously larger than those of **3**, **4**, and **5**, which means **1** and **2** have the stronger electron injection abilities than the other complexes. In addition, the reorganization energies for electron transport ($\lambda_{electron}$) and reorganization energies for hole transport ($\lambda_{hole}$) have been clarified in the previous article [28]. From the calculated data in Table 2, it can be seen that the complex **3** has the best hole transfer ability with the smallest $\lambda_{hole}$ value (0.228 eV) among these complexes. The $\lambda_{electron}$ values for complexes **1**−**5** are larger than the $\lambda_{hole}$ values, which suggests that the hole transfer rate is better than the electron transfer rate. In addition, it can be seen that the difference between $\lambda_{electron}$ and $\lambda_{hole}$ for complex **3** is the smallest among these complexes, which can greatly improve the charge transfer balance, thus further enhancing the device performance of OLEDs. It can be seen that the charge transfer rate of holes and electrons for these complexes show evident change due to the introduction of electron-withdrawing and electron-donating substituted groups in the ancillary ligand

### *3.4. Absorption Spectra*

To gain insight into the absorption properties, the lowest 60 singlet excitation energies for complexes **1**–**5** were calculated by TDDFT in $CH_2Cl_2$ medium on the basis of the optimized $S_0$ geometries. The vertical electronic excitation energies, oscillator strengths ($f$), assignment, and configurations have been listed in Table S6 (Supplemental material). The absorption spectra of the studied complexes are shown in Fig. 3.

As shown in Table S6, the lowest lying $S_0 \rightarrow S_1$ absorption wavelengths are located at 362 nm ($f = 0.1102$) for **1**, 372 nm ($f = 0.1327$) for **2**, 361 nm ($f = 0.0801$) for **3**, 361 nm ($f = 0.0983$) for **4**, and 355 nm ($f = 0.1400$) for **5**, respectively. It can be seen that the calculated 361 nm absorption for **3** is in good agreement with the experimental values 367 nm [26]. Fig. 3 shows that complexes **1**, **3**, and **4** have the largest absorption peaks at about 266 nm. However, complexes **2** and **5** have the largest absorption peaks at about 279 nm and the similar absorption shapes. In addition, complexes **1** and **2** have the absorption bands in the energy range from 350 to 375 nm. The lowest energy absorptions of **1** and **2** are characterized as MLCT (metal to ligand charge transfer)/LLCT (ligand to ligand charge transfer)/ILCT (intraligand charge transfer) [d(Pt)+$\pi$(C^N+dpmH)→$\pi^*$(C^N)].

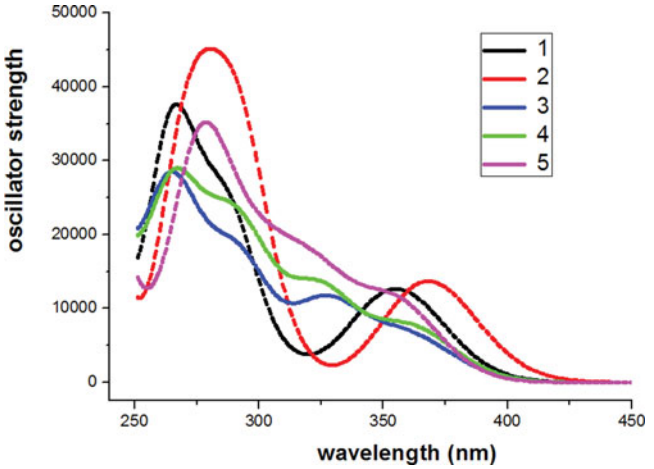


**Figure 3.** Simulated absorption spectra in $CH_2Cl_2$ medium for complexes **1**–**5**.

Nevertheless, the lowest energy absorptions of **3**, **4**, and **5** are characterized as MLCT/ILCT [d(Pt)+$\pi$(CˆN)→$\pi^*$(CˆN)].

### *3.5. Phosphorescence*

To check the computational method, two different density functionals (B3LYP and M062X) were used [29]. A good agreement with experimental data was obtained for M062X, while a disagreement was found for B3LYP. The calculated lowest energy emissions for the synthesized complexes **1** and **3** at B3LYP level are localized at 604 and 587 nm, respectively. However, the lowest energy emissions at M062X for **1** and **3** are 520 and 513 nm, respectively, which are in good agreement with the experimental data (537 and 528 nm) [26]. On the basis of the optimized $T_1$ structures, the emission wavelengths, emission energies, and transition nature of complexes **1**–**5** calculated by the M062X method in $CH_2Cl_2$ medium have been listed in Table 3.

Table 3 shows that the calculated lowest energy emissions of the five complexes are located at 520, 544, 513, 519, and 523 nm, respectively, which are dominantly controlled by the excitation of LUMO→HOMO. The emission transition characters of these complexes

**Table 3.** Phosphorescent emissions of complexes **1**–**5** in $CH_2Cl_2$ medium at the TDDFT/M062X levels, respectively, along with experimental wavelength (nm) available (H Indicates HOMO, L Indicates LUMO)

| | λ(nm)/*E*(eV) | Configuration | Nature | Exptl.[a] |
|---|---|---|---|---|
| **1** | 520/2.38 | L→H(84%) | $^3$MLCT/$^3$LLCT | 537 |
| **2** | 544/2.27 | L→H(88%) | $^3$MLCT/$^3$LLCT | |
| **3** | 513/2.41 | L→H(89%) | $^3$MLCT/$^3$LLCT | 528 |
| **4** | 519/2.38 | L→H(92%) | $^3$MLCT/$^3$LLCT | |
| **5** | 523/2.36 | L→H(94%) | $^3$MLCT/$^3$LLCT | |

[a]Ref. [26].

**Table 4.** The contribution of $^3$MLCT (%) in the $T_1$ state, the energy gaps between the $S_1$ and $T_1$ states ($\Delta E_{S_1-T_1}$) (in eV), and the transition electric dipole moment ($\mu_{S_1}$) in the $S_0 \rightarrow S_1$ transition for complexes **1**–**5**

| | $^3$MLCT | $\Delta E_{S_1-T_1}$ | $\mu_{S_1}$ | $\Phi^a$ |
|---|---|---|---|---|
| **1** | 23.5 | 0.94 | 1.31 | |
| **2** | 23.7 | 0.99 | 1.62 | |
| **3** | 24.9 | 0.94 | 0.95 | 0.08[a] |
| **4** | 23.0 | 0.94 | 1.16 | |
| **5** | 13.1 | 1.01 | 1.64 | |



are the $^3$MLCT (triplet metal to ligand charge transfer)/$^3$LLCT(triplet ligand to ligand charge transfer) characters. It can be seen that complex **2** has the largest emission wavelength 544 nm among these studied complexes. It is also noted that the lowest energy emissions of **1**, **2**, **4**, and **5** are red shift than that of complex **3**.

The emission quantum yield ($\Phi$) can be affected by the competition between $k_r$ (radiative decay rate) and $k_{nr}$ (nonradiative decay rate), i.e., $\Phi = k_r/(k_r + k_{nr})$. It can be seen, to increase the quantum yield, $k_r$ should be increased and $k_{nr}$ should be decreased simultaneously or respectively [30, 31]. In addition, $k_r$ is also theoretically related to the mixing between $S_1$ and $T_1$, which is proportional to the spin-orbit coupling (SOC) and inversely proportional to the energy gaps between the $S_1$ and $T_1$ states according to the following formula [32, 33]:

$$k_r \approx \gamma \frac{\langle \psi_{S_1} | H_{S_0} | \psi_{T_1} \rangle^2 \mu_{S_1}^2}{(\Delta E_{S_1-T_1})^2}$$
$$\gamma = 16\pi^3 10^6 n^3 E_{em}^3 / 3h\varepsilon_0 \quad (1)$$

Where $H_{S_0}$ is the Hamiltonian for the spin-orbit coupling, $\mu_{S_1}$ is the transition dipole moment in the $S_0 \rightarrow S_1$ transition, $\Delta E_{S_1-T_1}$ is the energy gaps between the $S_1$ and $T_1$ states, $E_{em}$ represents the emission energy in $cm^{-1}$, and $n$, $h$, and $\varepsilon_0$ are the refractive index, Planck's constant and the permittivity in a vacuum, respectively. Accordingly, the variation of quantum yield ($\Phi$) can be qualitatively analyzed in theory from the above formula.

A strong spin-orbit coupling by the central Pt atom leads to fast intersystem crossing (ISC) and efficient phosphorescence at room temperature. It is also known that the phosphorescence quantum efficiencies could be increased by a larger $^3$MLCT composition and thus the ISC. In Table 4, we have listed the $^3$MLCT contributions which were calculated to be 23.5%, 23.7%, 24.9%, 23.0%, and 13.1% for complexes **1**–**5**, respectively. The $\Delta E_{S_1-T_1}$ values for these complexes are 0.94, 0.99, 0.94, 0.94, and 1.01 eV, respectively. The $\mu_{S_1}$ values for these complexes are 1.31, 1.62, 0.95, 1.16, and 1.64 Debye, respectively. According to equation (1), it can be seen that a lower $\Delta E_{S_1-T_1}$, larger $^3$MLCT contribution and higher $\mu_{S_1}$ value may account for a larger $k_r$. From the data in Table 4, it can be seen that the complex **2** the larger $k_r$ value than those of other complexes.

## 4. Conclusions

Briefly summarizing the above, we have adopted DFT and TDDFT methods to investigated the geometrical and electronic structures, absorption and emission properties, charge injection and transport performance, and phosphorescence efficiency of a series of platinum(II) complexes with different substituent group (–$CF_3$, –CN, –H, –$CH_3$, and –$OCH_3$) in the C^N cyclometalating ligand. It can be seen that the electron-withdrawing and electron-donating substituted groups in the C^N cyclometalating ligand have the obvious effect on the photophysical properties, such as absorption and emission spectra, electron injection and transport abilities. The lowest energy emissions of the five complexes are located at 520, 544, 513, 519, and 523 nm, respectively, which are dominantly controlled by the excitation of LUMO→HOMO with the $^3$MLCT/$^3$LLCT transition characters. It can be also predicted that the complex **2** possibly owns the largest $k_r$ value among the five complexes. We hope that this study can be helpful to provide constructive information for designing novel platinum(II) OLEDs materials in the future.



## Funding

The authors are grateful to the financial aid from the Program of Science and Technology Development Plan of Jilin Province of China (Grant Nos. 20140520090JH, 20130206032YY), the Science and Technology Research Project for the Twelfth Five-year Plan of Education Department of Jilin Province of China (Grant No. 2014–37), the Fund for Doctoral Scientific Research Startup of Changchun University of Science and Technology (Grant No. 40301855), and the Science and Technology Innovation Fund of Changchun University of Science and Technology (Grant No. XJJLG-2014-12).

## References

[1] Jia, W. L. *et al.* (2004). *Chem. Eur. J.*, *10*, 994.
[2] Slinker, J. D. *et al.* (2004). *J. Am. Chem. Soc.*, *126*, 2763.
[3] Mazzeo, M. *et al.* (2005). *Adv. Mater.*, *17*, 34.
[4] Yang, C. H. *et al.* (2005). *Inorg. Chem.*, *44*, 7770.
[5] Lowry, M. S., & Bernhard, S. (2006). *Chem. Eur. J.*, *12*, 7970.
[6] Yersin, H. (Ed.). (2008). *Highly Efficient OLEDs with Phosphorescent Materials*, Wiley-VCH: Weinheim, Germany.
[7] Wong, W. Y., & Ho, C. L. (2009). *J. Mater. Chem.*, *19*, 4457.
[8] Kamtekar, K. T., Monkman, A. P., & Bryce, M. R. (2010). *Adv. Mater.*, *22*, 572.
[9] Shang, X. H., Han, D. M., Li, D. F., & Wu, Z. J. (2013). *Chem. Phys. Lett.*, *565*, 12.
[10] Yang, X. L., Yao, C. L., & Zhou, G. J. (2013). *Platinum Metals Rev.*, *57*, 2.
[11] Baldo, M. A. *et al.* (1998). *Nature*, *395*, 151.
[12] Lu, W. *et al.* (2002). *Chem. Commun.*, 206.
[13] Lu, W. *et al.* (2004). *J. Am. Chem. Soc.*, *126*, 4958.
[14] Unger, Y., Zeller, A., Ahrens, S., & Strassner, T. (2008). *Chem. Commun.*, 3263.
[15] Feng, K. *et al.* (2009). *Macromolecules*, *42*, 6855.
[16] Adamovich, V. *et al.* (2002). *New J. Chem.*, *26*, 1171.
[17] Zhou, G. J., Wong, W. Y., Yao, B., Xie, Z., & Wang, L. (2008). *J. Mater. Chem.*, *18*, 1799.
[18] Ho, C. L., Wong, W. Y., Yao, B., Xie, Z., Wang, L., & Lin, Z. (2009). *J. Organomet. Chem.*, *694*, 2735.
[19] Wu, W. *et al.* (2010). *Eur. J. Inorg. Chem.*, 4683.
[20] Rao, Y. L. *et al.* (2012). *Chem. Eur. J.*, *18*, 11306.
[21] Shigehiro, T. *et al.* (2013). *J. Phys. Chem. C*, *117*, 532.

[22] Brooks, J. *et al.* (2002). *Inorg. Chem.*, *41*, 3055.
[23] Adamo, C., & Barone, V. (1999). *J. Chem. Phys.*, *110*, 6158.
[24] O′Boyle, N. M., Tenderholt, A. L., & Langner, K. M. (2008). *J. Comput. Chem.*, *29*, 839.
[25] Frisch, M. J. *et al.* (2009). *Gaussian 09*, Gaussian, Inc.: Wallingford, CT.
[26] Kourkoulos, D. *et al.* (2013). *Dalton Trans.*, *42*, 13612.
[27] Avilov, I., Minoofar, P., Cornil, J., & De Cola, L. (2007). *J. Am. Chem. Soc.*, *129*, 8247.
[28] Han, D. M., Zhang, G., Cai, H. X., Zhang, X. H., & Zhao, L. H. (2013). *J. Lumin.*, *138*, 223.
[29] Zhao, Y., & Truhlar, D. G. (2008). *Theor. Chem. Acc.*, *120*, 215.
[30] Fantacci, S., De Angelis, F., Sgamellotti, A., Marrone, A., & Re, N. (2005). *J. Am. Chem. Soc.*, *127*, 14144.
[31] Tamayo, A. B. *et al.* (2005). *Inorg. Chem.*, *44*, 8723.
[32] Haneder, S. *et al.* (2008). *Adv. Mater.*, *20*, 3325.
[33] Turro, N. J. (2002). *Modern Molecular Photochemistry*, University Science Books: Palo Alto, USA.